Article

Discovery Medicine 2025; 37(200): 1800–1814
https://doi.org/10.24976/Discov.Med.202537200.156

TES7832-Mediated Selective Inhibition of the Scavenger Receptor Cysteine-Rich Domain of the Transmembrane Protease Serine 2/ERG Gene Fusion—A Novel and Potential Approach for Suppressing the ERG-Driven Prostate Cancer

Majed Al Fayi[1], Ayed A. Dera[1,*]

[1]Department of Clinical Laboratory Sciences, College of Applied Medical Sciences, King Khalid University, 61421 Abha, Saudi Arabia
*Correspondence: ayedd@kku.edu.sa (Ayed A. Dera)
Submitted: 21 March 2025 Revised: 29 April 2025 Accepted: 14 May 2025 Published: 20 September 2025

Background: The Transmembrane Protease Serine 2/ERG (*TMPRSS2/ERG*) gene fusion results in the overexpression of *ERG* and dysregulation of pathways critical for prostate cancer (PC) tumor progression, invasion, and metastasis. This study aims to target the *TMPRSS2/ERG* fusion in the Scavenger Receptor Cysteine-Rich (SRCR) domain presents a promising and novel therapeutic strategy to control the aggression of PC malignancy. The study aims to identify targeted novel small molecules against the TMPRSS2 protein for lead identification and validation.

Methods: High-throughput virtual screening (HTVS) against the ChemBridge library was followed by protein-ligand interaction profilers, GROMACS, and GMX_Molecular Mechanics Poisson-Boltzmann Surface Area (MMPBSA) techniques were used for the lead identification. VCaP, LNCaP, human umbilical vein endothelial cells (HUVEC), and RWPE-1 cells were involved in the *in vitro* validations.

Results: HTVS identified TES7832 with favorable binding affinities of –8.0 kcal/mol to the SRCR domain of TMPRSS2. Molecular dynamic simulations demonstrated stable binding interactions with Root Mean Square Deviation values around 0.15 nm. The ΔG binding calculation was –36.76 kcal/mol (mean $\pm$ 5.63 standard deviation). Absorption, Distribution, Metabolism, Excretion, and Toxicity (ADMET) supported favorable small-molecule characteristics. TES7832 inhibited TMPRSS2 activity dose-dependently with a half-maximal inhibitory concentration (IC_{50} value) of 484.1 $\pm$ 21.88 nM. The compound was selective to control the proliferation of VCaP cells expressing the *TMPRSS2/ERG* gene fusion with a 50% growth inhibition concentration (GI_{50}) value of 392 $\pm$ 39.15 nM. TES7832 reduced *ERG* and androgen receptor (AR) positive populations of VCaP cells while sparing the LNCaP or HUVEC cells that do not possess *TMPRSS2/ERG* fusion. The compound favored apoptosis and G_2/M cell cycle arrest in VCaP cells and inhibited hepatocyte growth factor (HGF)-induced transmigration of these cells.

Conclusion: TES7832 targeted the SRCR domain of the *TMPRSS2/ERG* fusion to downregulate *ERG* and AR activity in PC cells to control proliferation and induce apoptosis. This selectivity of TES7832 warrants further preclinical developments of the molecule against the *TMPRSS2/ERG* fusion-driven PC malignancy.

Keywords: prostate cancer; *TMPRSS2/ERG*; gene fusion; high throughput virtual screening; apoptosis

Introduction

Prostate cancer (PC) remains one of the most frequently diagnosed cancers in men, with approximately 1.4 million new cases and 375,000 deaths reported worldwide in 2020, making it the second most commonly diagnosed cancer in men [1]. While advancements in treatments have improved outcomes for early-stage disease, therapeutic options for advanced and metastatic prostate cancer remain limited [2,3]. A significant proportion of prostate cancers is driven by genetic alterations, including the Transmembrane Serine Protease 2/ERG (*TMPRSS2/ERG*) gene fusion, which promotes aggressive disease progression and resistance to standard therapies. This fusion event, characterized by the aberrant expression of the *ERG* oncogene under the control of the TMPRSS2 promoter, has emerged as a crucial molecular target in prostate cancer [4–6].

The TMPRSS2 plays an essential role in normal physiological processes and disease pathogenesis, particularly in PC characterized by the *TMPRSS2/ERG* gene fusion [7]. The *TMPRSS2/ERG* gene fusion is one of the most common genetic alterations in prostate cancer, occurring in approximately 40–50% of cases, particularly among patients of European descent [8]. This fusion event is associated with disease progression and has been linked to a more aggressive tumor phenotype in certain subgroups [9]. While

its presence alone is not directly predictive of recurrence or mortality, studies have shown that *TMPRSS2/ERG*-positive tumors may have a higher risk of biochemical recurrence, especially when combined with other molecular alterations [10]. Structurally, TMPRSS2 consists of two critical domains: the N-terminal Scavenger Receptor Cysteine-Rich (SRCR) domain and the C-terminal serine protease domain [11]. The SRCR domain, often overlooked in therapeutic studies, plays a pivotal role in ligand binding and regulatory interactions that influence the proteolytic activity of TMPRSS2 [11]. Given its involvement in key protein-ligand interactions and its potential to modulate downstream signaling events, the SRCR domain represents an attractive but underexplored target for therapeutic intervention [12].

Despite the importance of the SRCR domain, most drug discovery efforts have focused on targeting the serine protease activity of TMPRSS2 [13]. However, inhibiting the SRCR domain offers a novel approach to disrupting TMPRSS2 function in prostate cancer, particularly in cases where the *TMPRSS2/ERG* fusion drives disease progression. Targeting this domain may provide a dual benefit by interfering with ligand recognition and protease activation, offering a more comprehensive strategy for inhibiting TMPRSS2-mediated pathways [14]. Given the structural complexity of the SRCR domain and its critical role in ligand interactions, computational and structure-based drug discovery approaches are essential to identify selective inhibitors.

In this study, we employed a structure-based drug discovery approach to target the SRCR domain of TMPRSS2. High-throughput virtual screening of a diverse chemical library was combined with molecular docking and Absorption, Distribution, Metabolism, Excretion, and Toxicity (ADMET) property evaluation to identify promising lead compounds. Molecular dynamics simulations and binding free energy calculations further characterized the interactions and stability of the protein-ligand complexes. By focusing on the SRCR domain, our work provides a novel framework for therapeutic development targeting TMPRSS2, with potential implications for prostate cancer treatment.

Materials and Methods

Structure Retrieval and High-Throughput Virtual Screening

To identify potential ligands for TMPRSS2, a virtual screening campaign was conducted using the Diversity-based High-throughput virtual screening (D-HTVS) technique from the SiBioLEAD platform (https://sibiolead.com/). D-HTVS performs two-stage docking, viz., stage 1 docking with scaffolds, followed by stage 2 docking with chemically related compounds of the top 10 scaffolds identified in stage 1 docking. A ChemBridge database comprising approximately 850,000 compounds (350–750 kDa) was selected for analysis. The TMPRSS2 full-length protein structure was obtained from the AlphaFold database (https://alphafold.ebi.ac.uk/entry/O15393) and processed using a standard preparation workflow to optimize its geometry for docking studies, including removal of disordered regions from amino acids 1 to 115. For docking studies, amino acid residues 116 to 492 were kept. Filtering criteria, including molecular weight between 350 and 750 Da and adherence to Lipinski's Rule of Five, were applied to narrow down the compound set. Docking simulations were executed using the integrated Autodock-Vina tool, version 1.1.2 (Scripps Research Institute, San Diego, CA, USA), to predict favorable binding interactions.

GROMACS-Based Molecular Dynamics Simulation (MDS)

To further evaluate the binding properties and stability of the top-scoring ligands from the virtual screening, molecular dynamics (MD) simulations were performed with GROMACS, Version 2021, on the SiBioLEAD platform (https://sibiolead.com/). The protein-ligand complexes were solvated within a triclinic box containing Simple Point Charge (SPC) water molecules to simulate a physiological environment. Sodium chloride was introduced at a concentration of 0.15 M to mimic ionic conditions and maintain system neutrality. Energy minimization was initially conducted using the steepest descent method to eliminate steric clashes and optimize the system. A dual-phase equilibration process was then carried out over 300 ps to stabilize the configuration under constant temperature and pressure. MD simulations were subsequently run for 100 ns, capturing trajectory data for comprehensive analysis. Metrics, including Root Mean Square Deviation (RMSD), were calculated to assess protein-ligand complex stability, and hydrogen bond interactions were monitored to gauge the consistency of binding.

Molecular Mechanics Poisson-Boltzmann Surface Area (MM-PBSA)

The binding affinity of the ligands was quantified using Molecular Mechanics Poisson-Boltzmann Surface Area (MM-PBSA) calculations. Fifty representative frames were extracted from the 100-ns MD simulation trajectories for analysis. The GMX_ Molecular Mechanics Poisson-Boltzmann Surface Area (MMPBSA) tool [15], available through the SiBioLEAD platform, was employed to calculate free energy contributions encompassing van der Waals forces, electrostatics, polar solvation, and non-polar solvation effects. Average binding free energy values were computed from the sampled frames, allowing for the identification of ligands with strong binding affinities. Compounds with highly favorable energy scores were prioritized for further investigation.

ADMET Profiling

ADMET properties were assessed using the ADMET-AI tool (https://admet.ai.greenstonebio.com/) [16]. The ligands were converted to SMILES format for compatibility with the web server and uploaded for analysis. The tool provided detailed predictions for pharmacokinetic parameters, including absorption efficiency, metabolic stability, distribution patterns, and potential toxicity risks. Graphical outputs facilitated the comparison of ADMET profiles, enabling the selection of drug candidates with optimal properties. This evaluation was crucial in prioritizing compounds for experimental validation based on their predicted safety and pharmacological characteristics.

TMPRSS2 Inhibition Assay

The cell-free TMPRSS2 assay was carried out using the fluorogenic kit method (TMPRSS2 inhibition kit # 78083BPS Bioscience, San Diego, CA, USA) as per the manufacturer's instructions. Briefly, the assay was initiated by the addition of 10 µL of the Log dilutions (ranging from 0.1 nM to 10,000 nM) of TES7832 (# 5310483, ChemBridge, San Diego, CA, USA) or camostat (# SML0057, Sigma Aldrich, St. Louis, MO, USA) at the destinated final concentrations to the test wells, while the blank received 10 µL of diluent solution. Following this, 30 µL/well of TMPRSS2 diluted in the 1X buffer (5 ng/µL) was added to the 96-well plates. The blank well was added with 30 µL of 1X buffer. The plate was incubated for 30 minutes at room temperature. The kinase reaction was initiated by adding 10 µL of TMPRSS2 substrate (50 µM) to all wells. The plate was kept away from the light and incubated for 10 minutes at room temperature. Fluorescence was read at 380 nm excitation and 450 nm emission using a FLUOstar Omega microplate reader (BMG LABTECH, Cary, NC, USA). Blank values were subtracted, and the percentage inhibition of kinase activity was calculated and analyzed using GraphPad Prism software (version 6.0; GraphPad Software Inc., La Jolla, CA, USA). Half-maximal inhibitory concentration (IC_{50} values) was presented.

Cell Culture

VCaP (#CRL-2876, ATCC, Rockville, MD, USA), LNCaP (#CRL-1740, ATCC, Rockville, MD, USA), human umbilical vein endothelial cells (HUVEC) (#PCS-100-013, ATCC, USA), and RWPE-1 (adult normal prostate tissue-derived epithelial cells, #CRL-3607, ATCC, USA) were cultured in RPMI-1640 media with 10% FBS, 100 U/mL of penicillin, and 100 U/mL of streptomycin. The cells were passaged fewer than 6 months after resuscitation and were used for passage at an eighty percent confluency state. All prostate cancer cell lines used in this study were authenticated by short tandem repeat (STR) profiling and routinely tested for mycoplasma contamination using PCR-based assays. Only mycoplasma-free and STR-validated cells were used for all experimental procedures.

Cell Proliferation Assay

The MTT assay was used to assess proliferation as described elsewhere [17]. Briefly, VCaP, LNCaP, and RWPE-1 cells were seeded in 96-well plates (5×10^3 cells/well) and treated with Log dilutions (ranging from 0.1 nM to 10,000 nM) of TES7832 for 72 hours. Followingly, the cells were added with 1 mg/mL MTT (#M2003, Sigma Aldrich, USA), incubated for 4 h, and dissolved in DMSO. The purple formazan product formed was measured at 560 nm for absorbance using the FLUOstar Omega plate reader (BMG Labtech, Ortenberg, Germany). The percentage inhibition of cell proliferation was analyzed using the GraphPad Prism 6.0 software to determine the 50% growth inhibition concentration (GI_{50}) values.

Flow Cytometry

The *ERG* and androgen receptor (AR) signaling in PC cells was analyzed by flow cytometry. VCaP [TMPSSR2(+)/*ERG*-(+)/AR (+)] was treated with 200 nM, 400 nM, and 800 nM of TES7832 to enumerate dose response based on the near GI_{25}, GI_{50}, and GI_{100} values. LNCaP [TMPSSR2(+)/*ERG*-(-)/AR (+)] or HUVEC [TMPSSR2(-)/*ERG*-(+)/AR (+)] were treated with 10,000 nM of TES7832. All cells were incubated for 6 h in a 37 °C, CO_2 incubator. The cells were removed from the plates and transferred to sterile Eppendorf tubes. The cells were fixed with 4% formaldehyde for 10 minutes and then permeabilized with 90% methanol at –20 °C for 15 minutes. The cells were then incubated in 1X HBSS buffer/10% normal goat serum to block non-specific protein-protein interactions, followed by staining with 0.25 mg/mL of rabbit monoclonal PE-conjugated Anti-*ERG* antibody (EPR3864, #ab314261, Abcam, Waltham, MA, USA) or a 1:50 dilution of anti-androgen receptor (AR) rabbit monoclonal Ab, PE-Conjugated (#8428, Cell Signaling Technologies, Beverly, MA, USA) for thirty minutes in the dark. After two washes to remove the extra dye, the cells were suspended in the HBSS buffer. Guava EasyCyteTM flow cytometer (0500-5005, Merk Millipore, Madison, WI, USA), was used to acquire 5000 events. Analysis was carried out using InCyte software from Millipore (Burlington, CA, USA), to enumerate the percentage of positive populations of *ERG* or AR in all cell types, which were compared against the controls.

Annexin V Assay

VCaP cells were treated with 200 nM, 400 nM, and 800 nM of TES7832 for 48 hours to test the dose dependency in the apoptosis assay. Following the incubation period, the cells were washed using the kit's buffer and stained for 15 minutes in the dark using 0.25 µg/mL Annexin V reagent (# V13242, Thermo Scientific, Waltham, MA, USA). The cells were resuspended in a kit solution containing 0.5 µg/mL propidium iodide after two further washes. Flow cytometry was conducted by acquiring data

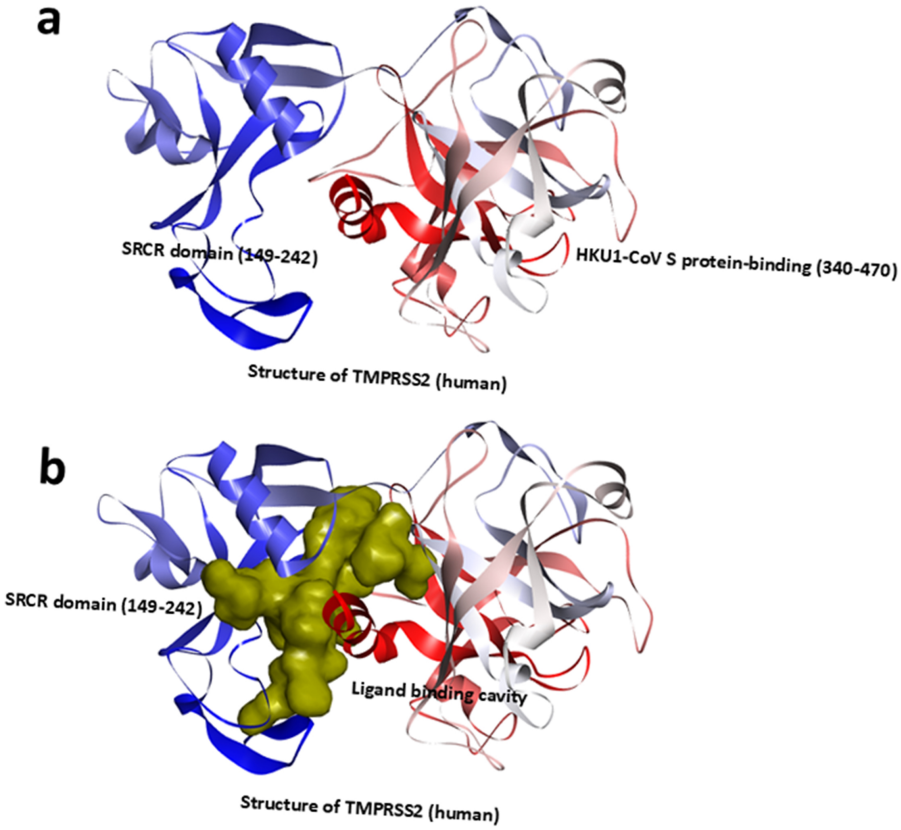

Fig. 1. Structure of Transmembrane Protease Serine 2 (TMPRSS2). (a) Full-length structure of TMPRSS2 protein retrieved from AlphaFold database, colored from N-terminal (blue) to C-terminal (red), showing the presence of two critical domains, Scavenger Receptor Cysteine-Rich (SRCR) (N-terminal), and CoV S protein binding domain (C-terminal) using the integrated Autodock-Vina tool (version 1.1.2 ; Scripps Research Institute, San Diego, CA, USA). (b) Ligand binding cavity prediction depicting the presence of a pocket at the N-terminal region (molecular surface representation), covering the SRCR domain.

from 10,000 events using a Guava EasyCyte™ flow cytometer (0500-5005, Merk Millipore, Madison, WI, USA), and the results were analyzed with InCyte software, Merck Millipore, WI, USA) to distinguish between healthy and apoptotic cells (early and late phase apoptosis). The findings were presented using GraphPad Prism software (version 6.0; La Jolla, CA, USA).

HGF-Stimulated Trans Migration Assay

The assay was carried out using a calorimetry-based kit (QCM™ Tumor Cell Trans-Endothelial Migration Assay kit (#ECM558, Merk Millipore, Madison, WI, USA) as per the manufacturer's instructions. Briefly, 1×10^5 of VCaP cells starved overnight in a serum-free medium were transferred to the pre-grown inserts with a monolayer of the HUVEC cells. VCaP cells were treated with 200 nM, 400 nM, and 800 nM of TES7832 and incubated for 1 hour in a CO_2 incubator. The inserts were then transferred to new wells with cell growth media containing 50 ng/mL hepatocyte growth factor (HGF) (Sigma Aldrich # 214-275-1). The PC cells were now allowed to migrate across the HUVEC membrane for 12 hours in a CO_2 incubator. Following, the inserts were removed from the wells and stained for 15 minutes using the staining solution provided in the kit. Furthermore, the stain was eluted using the kit elution buffer and read for absorbance at 570 nm using the FLUOstar Omega plate reader (BMG Labtech, Ortenberg, Germany). The percentage inhibition of the VCaP cell migration across the HUVEC membrane was calculated with respect to the control and presented.

The percentage of inhibition was calculated using optical density (OD) by the following formula: $(1 - (\text{Sample OD}/\text{Control OD})) \times 100$.

Cell Cycle Analysis

Following the manufacturer's instructions, the cell cycle assay was performed using the kit method. 200 nM, 400 nM, and 800 nM of TES7832 were added to VCaP cells at a density of 5×10^5 cells per well in a 6-well plate, and then the cells were incubated for 72 hours. 50 µL of Guava cell cycle reagent (#4500-0220, Merck Millipore, WI, USA) was added after two PBS washes, followed by a 15-minute dark incubation period, two wash buffer washes, and a resuspension in HBSS buffer. Guava EasyCyte™ flow cy-

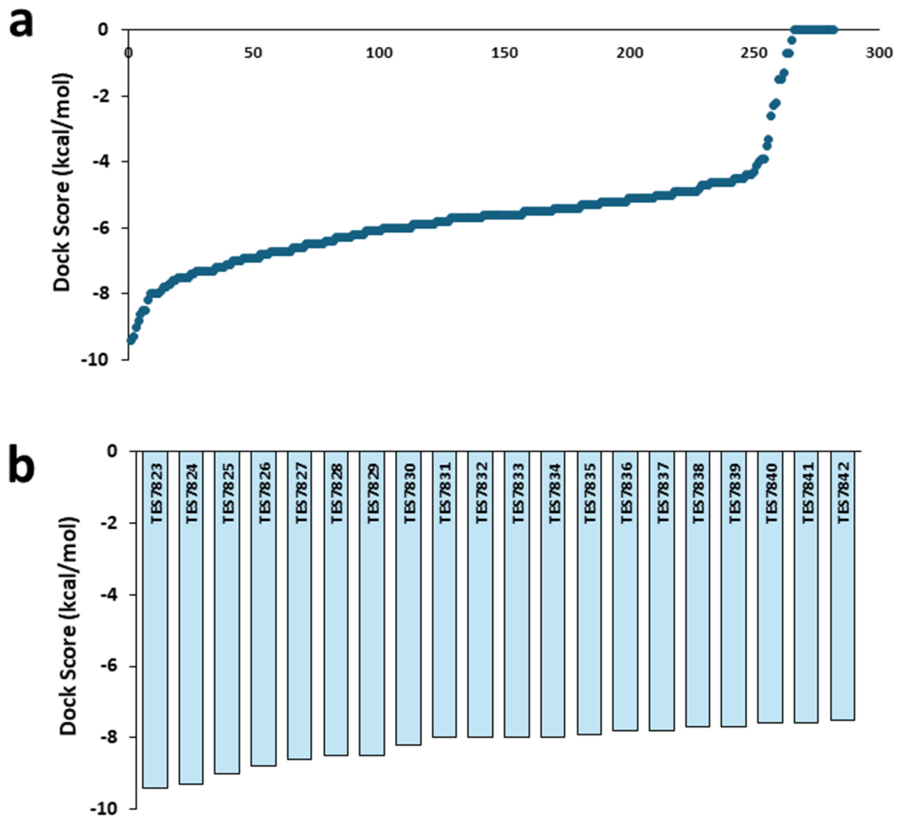

Fig. 2. High-throughput Virtual Screening of ChemBridge library. (a) Histogram representation of predicted docking scores for ChemBridge compounds, ranked based on binding energy, to the TMPRSS2 SRCR domain. (b) Histogram representation of the top 20 compounds ranked based on the docking energies.

tometer (0500-5005, Merk Millipore, Madison, WI, USA) was used to collect 10,000 events, and ExpressPro software (Burlington, CA, USA) was used to analyze the data. Results show the proportion of cell populations in each stage of the cell cycle.

Statistical

All experiments were performed in triplicate, and data were expressed as mean ± standard deviation (SD). Statistical analysis was conducted using GraphPad Prism software (version 6.0; La Jolla, CA, USA). GI_{50} and IC_{50} were calculated using a non-linear regression fit model with variable slope and plotted accordingly. Statistical difference was analyzed using one-way ANOVA (Analysis of Variance) followed by Tukey analysis. Statistical significance was set at $p < 0.05$.

Results

Structure Analysis of TMPRSS2

Toward identifying the best possible lead compound binding to the SRCR domain of TMPRSS2, the 3D structure of TMPRSS2 was retrieved. The full-length structure of TMPRSS2 retrieved from the AlphaFold database, which is processed by removal of disordered regions (1-115), revealed two critical domains, viz., the SRCR domain at the N-terminal and the CoV S protein binding domain at the C-terminal (Fig. 1a). Ligand binding cavity prediction identified a prominent pocket at the N-terminal region, primarily encompassing the entire SRCR domain (Fig. 1b).

High-Throughput Virtual Screening of ChemBridge Compounds Against the SRCR Domain of TMPRSS2 Protein

To identify the best lead molecule inhibitor of TMPRSS2, the whole ChemBridge library was screened against TMPRSS2. Screening of the ChemBridge library, containing compounds ranging from 350 kDa to 750 kDa against the SRCR domain of TMPRSS2 identified a wide range of compounds with favorable binding energies, as illustrated by the histogram distribution of docking scores (Fig. 2a). Among these, the top 20 compounds demonstrating significant favorable binding energies were chosen for further evaluation (Fig. 2b).

ADMET Property Prediction to Identify Top Lead Molecule Against TMPRSS2

Toward narrowing down the list of the top predicted compounds with favorable binding energies for further *in vitro* evaluation, ADMET properties were calculated. AD-

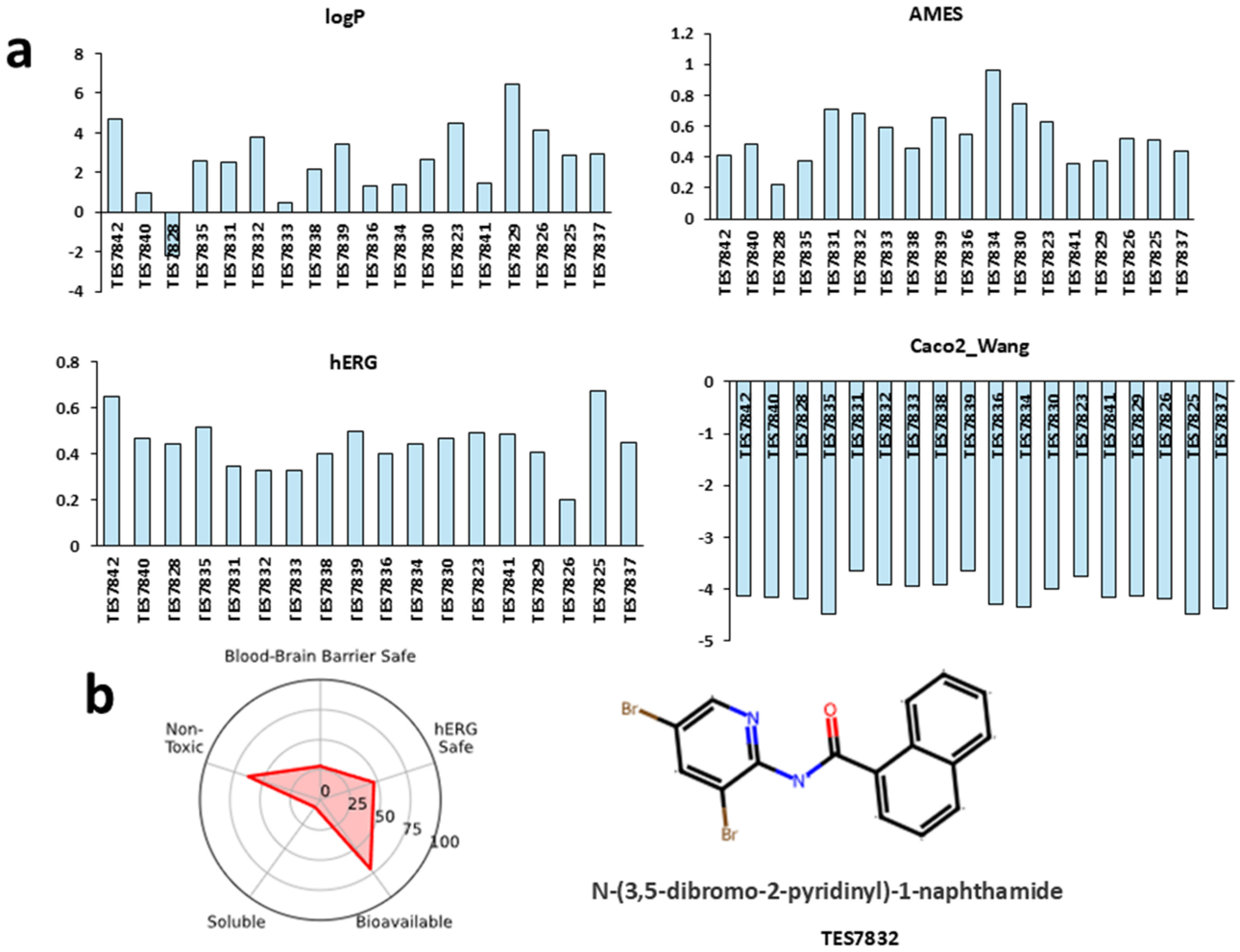

Fig. 3. Chemical Absorption, Distribution, Metabolism, Excretion, and Toxicity (ADMET) property prediction. (a) Histogram representation of ADMET-AI tool (https://admet.ai.greenstonebio.com/) predicted properties for the top 20 compounds, including logP, AMES, hERG, and Caco2_wang. (b) Predicted drug-like properties for the top compound TES7832.

MET property assessments for the top 20 compounds, using ADMET_AI, revealed favorable drug-like properties, including acceptable logP values, low toxicity potential (AMES test), potential for cardiotoxicity and arrhythmias (hERG), and permeability across Caco-2 cells (Fig. 3a). Based on these predictions, TES7832 (N-(3,5-dibromo-2-pyridinyl)-1-naphthamide) was identified as the top candidate with optimal predicted drug-like properties for further studies (Fig. 3b).

Protein-Ligand Interaction Analysis Identifies a Favorable Binding Pose for TES7832

Docking studies showed TES7832 bound firmly to the SRCR domain of TMPRSS2. Toward understanding the binding of the predicted lead molecule, TES7832, the protein-ligand complex was analyzed for its binding pose and interaction residues (Fig. 4a). Detailed interaction profiling highlighted multiple hydrogen bonds and hydrophobic contacts between TES7832 and key residues at the ligand-binding cavity (Fig. 4b). A 2D interaction map further confirmed the involvement of crucial amino acid residues in ligand binding. Key interactions include multiple hydrogen bonds and hydrophobic contacts with amino acid residues such as Arg150, Asp482, and Tyr485 of HUVEC cells at 10,000 nM, which are critical for stable ligand binding (Fig. 4c).

Molecular Dynamics Simulation of TMPRSS2: TES7832 Complex

Toward understanding the dynamics of the predicted lead molecule TES7832 when bound to the target protein TMPRSS2, a 100 ns Molecular Dynamic (MD) simulation was conducted, using the GROMACS simulation package available at SiBioLEAD LLC. MD simulation of the TMPRSS2:TES7832 complex revealed stable ligand interactions throughout the 100 ns trajectory. Snapshots of trajectory frames taken before and after the simulation show that the ligand-bound comfortably at the SRCR domain of the TMPRSS2 protein (Fig. 5a,b). RMSD analysis, which is a measure of quantifying the ligand binding stability over

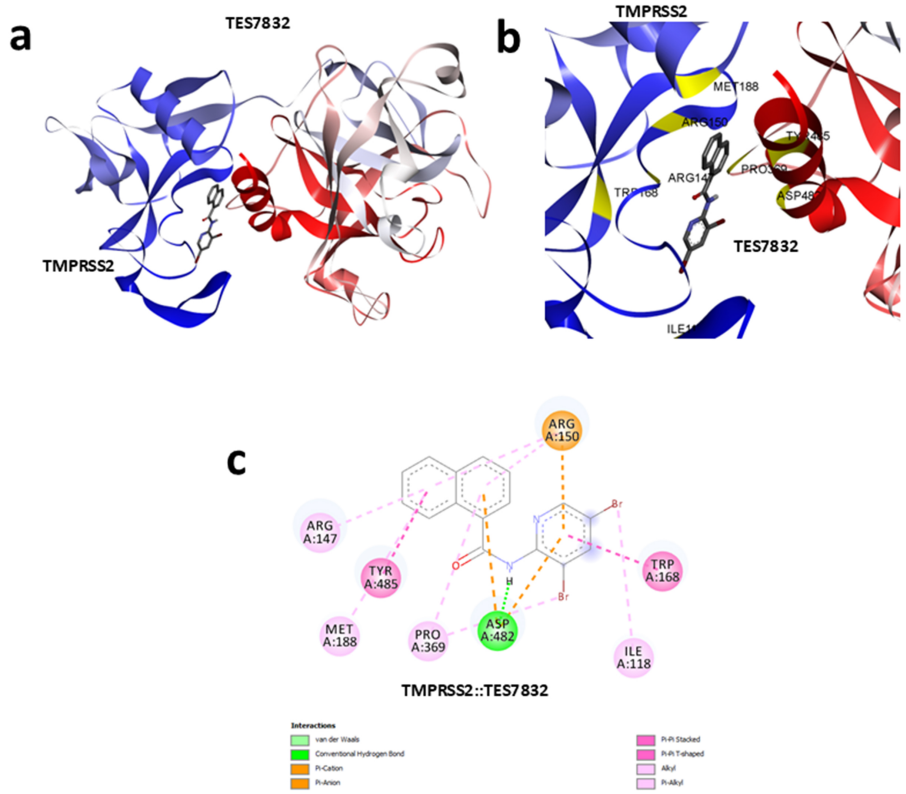

Fig. 4. Protein-ligand interaction analysis. (a) Predicted docking pose for the TES7832, showing ligand binding pose at the SRCR domain of the TMPRSS2 protein. (b) Protein-ligand interaction profiling showing the binding mode of TES7832 with amino acid residues at the predicted ligand-binding cavity of the TMPRSS2 protein. (c) 2D representation of protein-ligand interaction analysis showing amino acid residue interactions and the type of interactions with TES7832. Images were created using Discovery Studio Visualizer V2020 (Dassault Systèmes, San Diego, CA, USA).

time, confirmed minimal fluctuations, indicating a stable binding conformation throughout the 100 ns simulation period (Fig. 5c). Furthermore, the average protein-ligand hydrogen bonds calculated over the trajectory supported the stability of the interaction (Fig. 5d).

Binding Free Energy Estimation Identifies TES7832 Has a Favorable Binding Affinity Toward TMPRSS2

In order to calculate the binding free energy of TES7832 with TMPRESS2, MMPBSA-based binding free energy analysis was performed, using the GMX_MMPBSA package available in the SiBioLEAD LLC MD simulation module. MMPBSA-based binding energy estimation calculated from the 100 ns trajectory indicated a favorable Gibbs free energy for the TMPRSS2:TES7832 complex, –36.76 kcal/mol (mean ± 5.63 standard deviation), based on VDWAALS (van der Waals energy), which is nonbonded Lennard-Jones interactions, EEL (Electrostatic energy), which is Coulombic (charge-charge) interactions in vacuum, bond, angle, and dihedral, suggesting a strong and stable binding (Fig. 6).

TES7832 Inhibited the TMPRSS2 Activity and Controlled the VCaP Cell Proliferation

To augment the computational analysis of the lead compound, cell-free TMPRSS2 activity was tested. TES7832 dose-dependently inhibited the TMPRSS2 activity with an IC_{50} value of 484.1 ± 21.88 nM (Fig. 7a). The standard compound camostat exhibited an IC_{50} value of 4.72 ± 0.84 nM against the TMPRSS2 activity (Fig. 7b). To evaluate the translation of the TMPRSS2 inhibition at the cellular level, the antiproliferative effect of TES7832 was checked in VCaP and LNCaP cells. TES7832 inhibited VCaP cell proliferation with a GI_{50} value of 392 ± 39.15 nM (Fig. 8a). However, the compound did not make a change to the proliferating LNCaP cells. The viability of LNCaP cells was unaltered up to 10,000 nM of TES7832 treatment (Fig. 8b). Next, the effect of TES7832 on the HUVEC that express ERG was examined. There was no significant change in the viability of HUVEC cells with up to 10,000 nM TES7832 treatments (Fig. 8c). To check the effect of TES7832 on normal prostate cells, we tested the effect on the proliferation of RWPE-1 cells. The viability of these cells was not altered even at 10,000 nM TES7832 treatment (Fig. 8d).

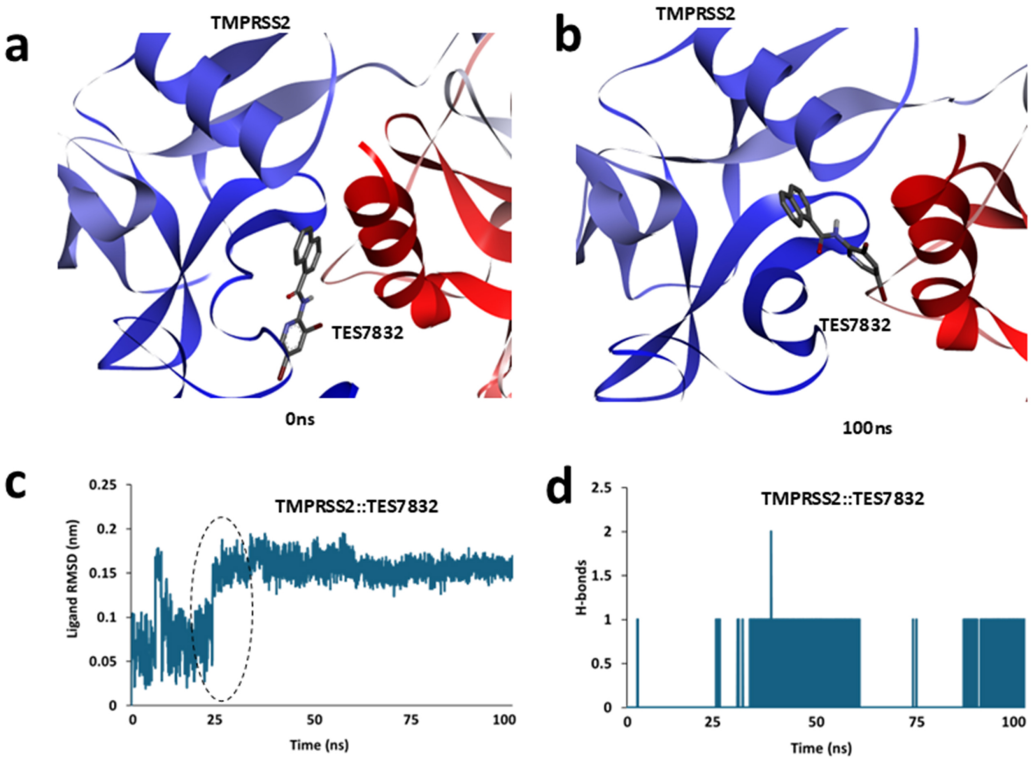

Fig. 5. Molecular dynamic simulation of protein-ligand complex. (a,b) Snapshot of trajectory frames at different time points, showing the stability of the ligand interaction. (c) Predicted ligand Root Mean Square Deviation (RMSD) calculated from 100 ns trajectory frames from TMPRSS2:TES7832. The black-dotted circle indicates the beginning of ligand stability. (d) Average protein-ligand h-bonds calculated from 100 ns simulation trajectories from TMPRSS2:TES7832. Images were created using Discovery Studio Visualizer V2020 (Dassault Systèmes, San Diego, CA, USA).

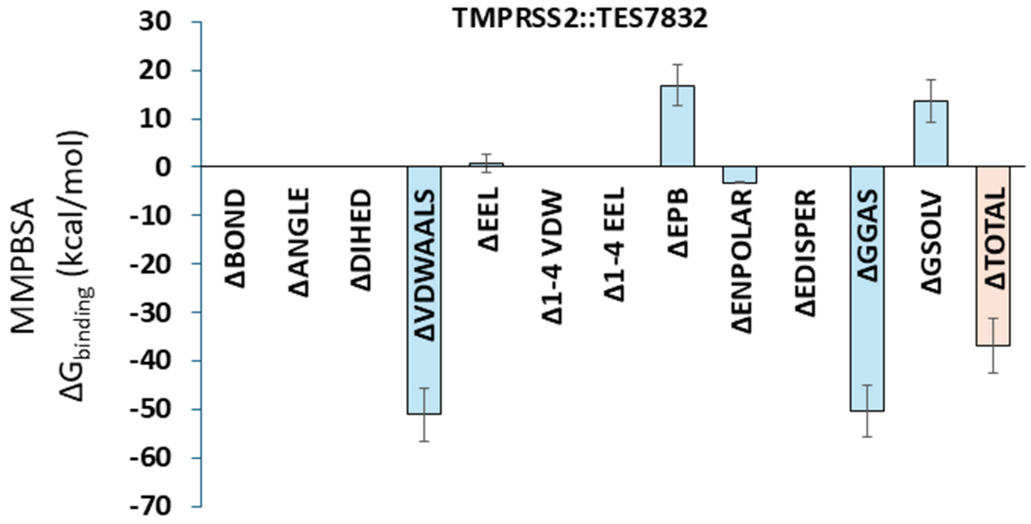

Fig. 6. Molecular Mechanics Poisson-Boltzmann Surface Area (MMPBSA)-based binding free energy estimate. Predicted Gibbs binding free energy estimate of 100 ns trajectory frames from TMPRSS2:TES7832 complex. Error bar represents mean ± standard deviation (SD). Δ, energy change; ANGLE, angle bending energy; DIHED, dihedral/torsional energy; VDWAALS, van der Waals energy; EEL, Electrostatic energy; 1-4 VDW, 1-4 van der Waals energy; EPB, polar solvation energy (Poisson–Boltzmann); ENPOLAR, nonpolar solvation energy; EDISPER, dispersion energy; GGAS, gas-phase energy; GSOLV, solvation free energy; TOTAL, total binding free energy.

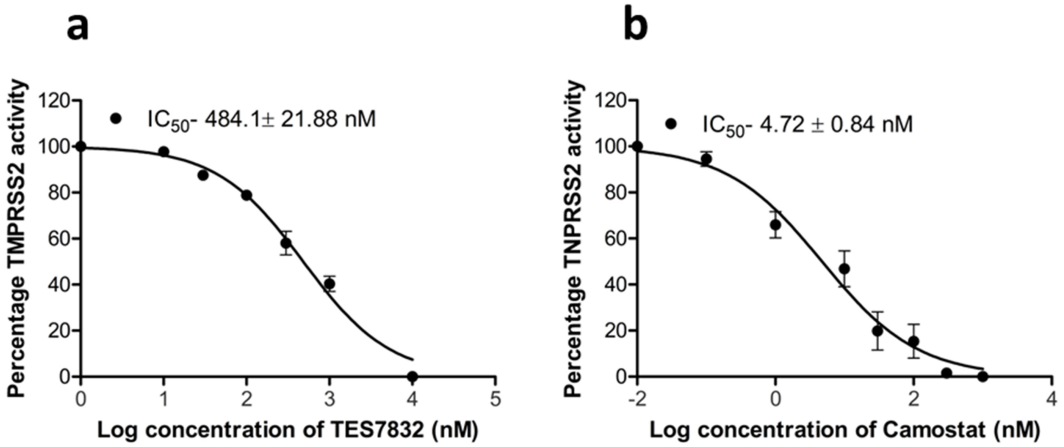

Fig. 7. Effect of TES7832 on TMPRSS2 activity. Variable concentrations (0.1 nM to 10,000 nM) of (a) TES7832 or (b) the standard compound camostat were tested against the TES7832 activity, and their half-maximal inhibitory concentration (IC_{50} values) were presented. Results expressed as mean ± SD from three experiments were analyzed using GraphPad Prism software (version 6.0; GraphPad Software Inc., La Jolla, CA, USA).

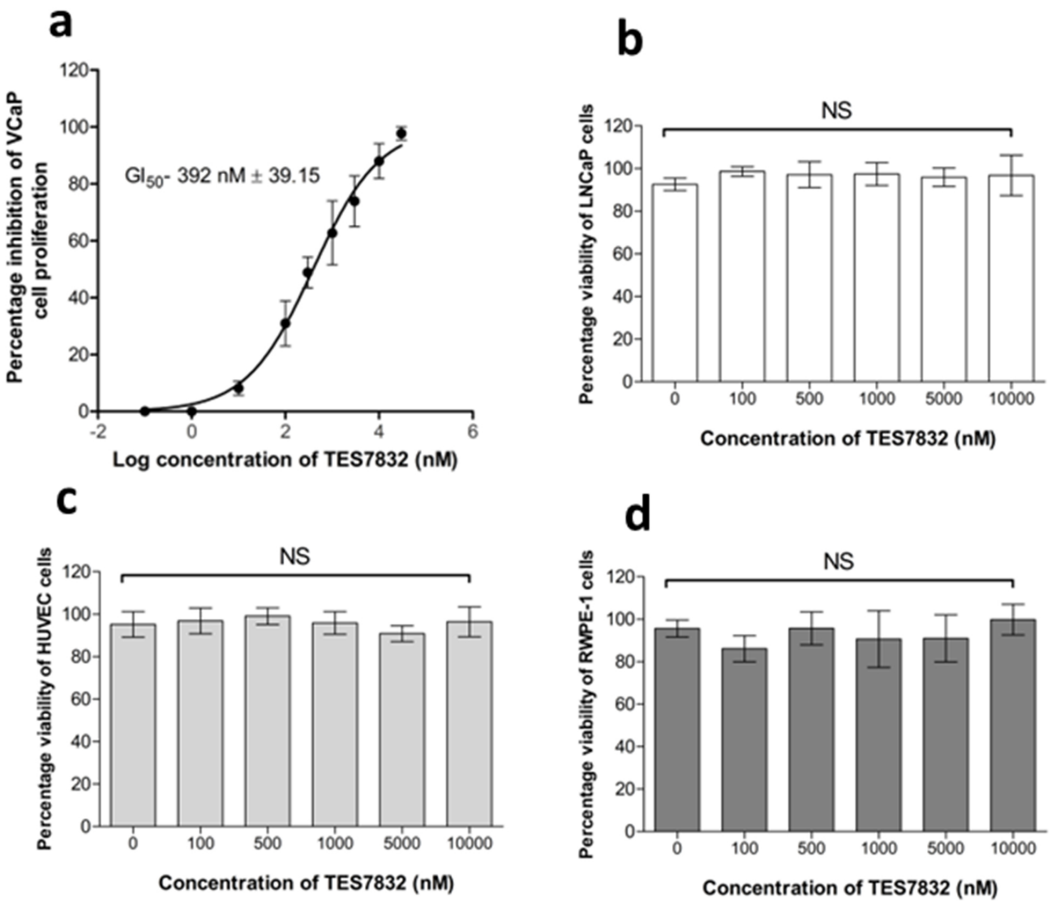

Fig. 8. Effect of TES7832 on cell growth/proliferation. The 50% growth inhibition concentration (GI_{50}) values of antiproliferative activity for TES7832 on (a) VCaP cells are presented. The compound was checked for its effect on the viability of (b) LNCaP, (c) human umbilical vein endothelial cells (HUVEC), and (d) RWPE-1 cells. TES7832 did not exhibit a significant change in the viability of these cells at the concentration range tested. The MTT assay was used to assess cell proliferation and viability, and mean ± SD values of percentage proliferation inhibition or cell viability were analyzed using GraphPad Prism version 6.0 software. NS, non-significant.

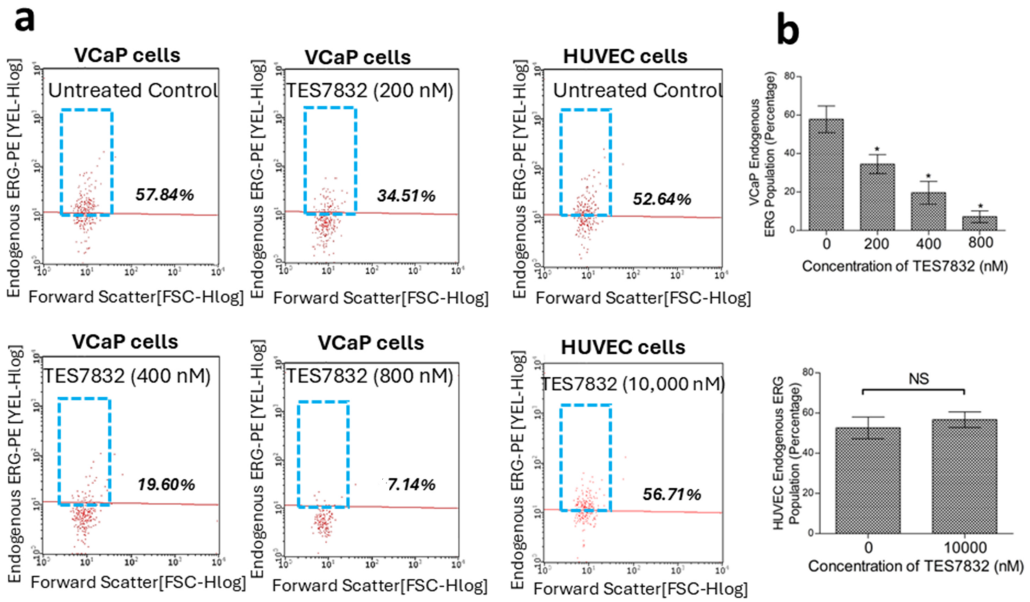

Fig. 9. TES7832 inhibited the *ERG*-positive population in selective cells. (a) TES7832 dose-dependently decreased the endogenous *ERG*-positive population in VCaP cells, while not affecting the levels of *ERG*-positive HUVEC cells at a much higher concentration. Representative graphs are depicted. (b) The numerical data are the average of three individual experiments. Statistical significance at * $p < 0.05$; NS, Non-significant.

TES7832 Attenuated ERG and AR in VCaP Cells

The effect of TES7832 on the endogenous *ERG*-positive populations of VCaP cells was tested. The compound dose-dependently decreased the *ERG*-positive population in VCaP cells (Fig. 9a). 200 nM treatment of TES7832 reduced the *ERG* population to 34.51 ± 4.91% from 57.8 ± 6.94% as that of the untreated control (Fig. 9b). Treatment of 400 nM and 800 nM of TES7832 further decreased these populations to 19.60 ± 5.88% and 7.14 ± 3.02%, respectively (Fig. 9b). The effect of TES7832 on endogenous *ERG* of HUVEC cells was also tested. The compound did not make a change to *ERG* populations of HUVEC cells at 10,000 nM (Fig. 9a,b). We tested the endogenous AR levels with TES7832 on VCaP, LNCaP, and HUVEC cells (Fig. 10a). Treatment with 200 nM TES7832 decreased the endogenous AR-positive population from 61.77 ± 7.10% to 33.00 ± 8.16% in VCaP cells, which further reduced to 21.61 ± 5.84% and 14.97 ± 6.66% in these cells with 400 nM and 800 nM TES7832 treatments, respectively (Fig. 10b). The endogenous AR levels of both HUVEC and LNCaP cells were not altered by the TES7832 treatment of 10,000 nM (Fig. 10b).

TES7832 Induced Apoptosis and Inhibited the HGF-Stimulated Migration, and Caused G_2/M Phase Accumulation of the VCaP Cell Cycle

Treatment with TES7832 enhanced the number of early and late-phase apoptotic cells in the VCaP cells, eventually increasing total apoptosis (Fig. 11a). TES7832 treatment at 200 nM, 400 nM, and 800 nM raised total apoptosis to 24.81 ± 3.55%, 35.73 ± 6.71%, and 45.10 ± 2.29% in VCaP cells, respectively, while the control exhibited 3.62 ± 1.77% of total apoptotic populations (Fig. 11b). Next, the antimetastatic efficacy of TES7832 in VCaP cells was tested by HGF-induced trans-endothelial cell migration assay. TES7832 dose-dependently inhibited the endothelial transmigration of VCaP cells across the HUVEC cell membrane under the influence of HGF (Fig. 11c). We then analysed the effect of TES7832 on the cancer cell cycle. When treated with TES7832, an increase in the G_2/M phase accumulation of the cell cycle was observed in the VCaP cells in dose dose-dependent way (Fig. 12a). TES7832 treatment at 200 nM, 400 nM, and 800 nM raised G_2/M phase population to 20.01 ± 4.68%, 31.67 ± 2.49%, and 36.48 ± 3.96% in VCaP cells respectively, while the control exhibited 10.07 ± 2.40% of total apoptotic populations (Fig. 12b).

Discussion

Prostate cancer remains one of the most prevalent malignancies among men, with significant challenges in identifying novel therapeutic targets [18]. One of the defining features of aggressive prostate cancers is the *TMPRSS2/ERG* gene fusion, which leads to aberrant expression of the *ERG* oncogene and promotes tumor progression [19]. Despite its clinical significance, targeting the *TMPRSS2/ERG* fusion has remained challenging due to the lack of druggable sites in *ERG* and the limited exploration of upstream regulatory elements like TMPRSS2 [20].

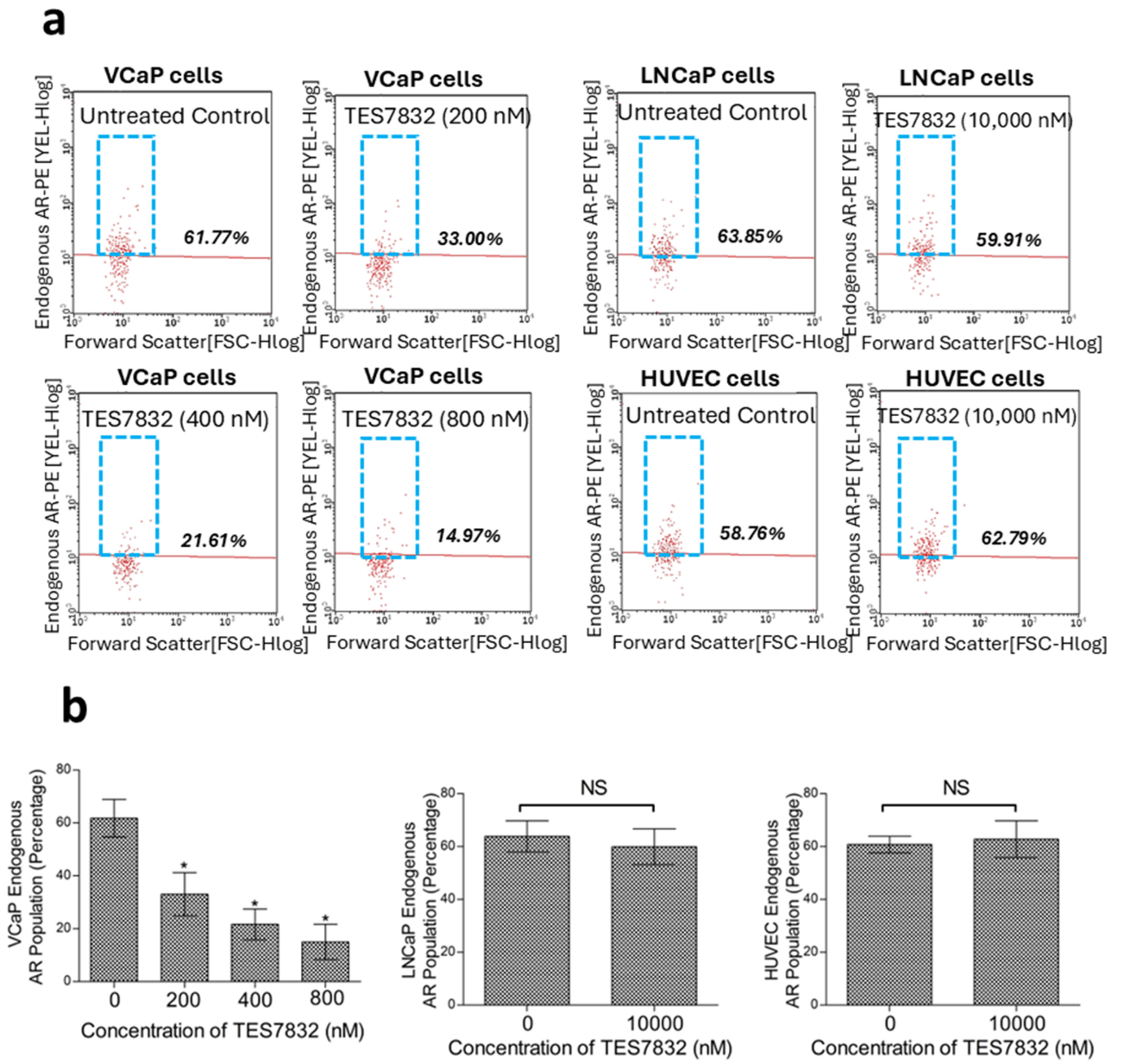

Fig. 10. TES7832 inhibited the androgen receptor (AR)-positive population in VCaP cells. (a) The effect of TES7832 was assessed in the VCaP, LNCaP, and HUVEC cells that express endogenous AR levels. Treatments with TES7832 dose-responsively inhibited the AR-positive populations in the VCaP cells, sparing the LNCAP and HUVEC cells. Representative graphs are depicted. (b) The numerical data are the averages from three individual experiments. Statistical significance at * $p < 0.05$; NS, Non-significant.

Given TMPRSS2's involvement in this fusion, its N-terminal SRCR domain emerges as a promising therapeutic target. In this study, structural analysis of TMPRSS2 identified a well-defined ligand-binding pocket within the SRCR domain. The SRCR domain in TMPRSS2 plays a crucial role in its interactions with other proteins, particularly in facilitating proteolytic activity essential for its biological functions. It is involved in recognizing and binding ligands, which is significant in mediating viral entry processes, such as those exploited by coronaviruses [21]. Targeting the SRCR domain offers therapeutic potential by inhibiting these critical interactions and disrupting TMPRSS2-related disease mechanisms, including prostate cancer [22]. This structural insight provided a rationale for conducting a high-throughput virtual screening of the ChemBridge library to identify potential lead inhibitors targeting this critical region.

Virtual screening identified a diverse set of compounds with favorable binding energies, from which the top 20 compounds were selected for further evaluation. ADMET property predictions streamlined the list, ultimately identifying TES7832 as the most promising lead. TES7832

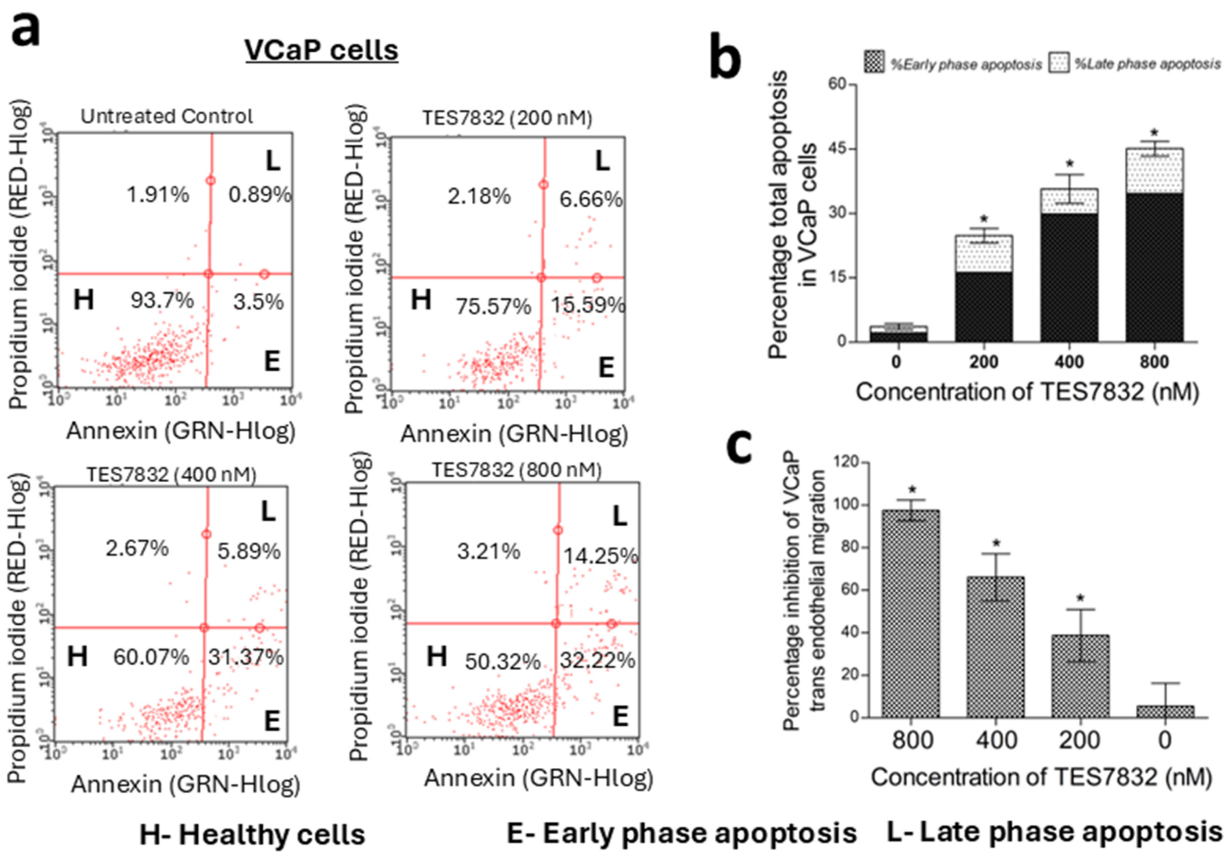

Fig. 11. Efficacy of TES7832 to promote apoptosis and inhibit hepatocyte growth factor (HGF)-mediated trans-endothelial migration. At 48 hours of treatment, the TES7832 promoted early and late-phase apoptosis in VCaP cells. (a) Representative graphs of the Annexin V assay depicting the induction of early and late apoptosis by TES7832 in the VCaP cells. (b) Histograms represent the dose-dependent efficacy of TES7832 in inducing early-phase, late-phase, and total apoptosis in VCaP cells. (c) TES7832 dose-dependently decreased the migration of VCaP cells across the HUVEC membrane under 50 ng/mL HGF influence. All tests were conducted three times, and representative results were provided. The results are expressed as mean ± SD and are statistically significant at $*p < 0.05$.

exhibited optimal drug-like properties, including acceptable solubility and minimal toxicity predictions, making it a strong candidate for further investigations.

Detailed protein-ligand interaction analysis revealed that TES7832 binds firmly within the SRCR domain, forming stable interactions with crucial residues, including ARG150, ASP482, and TYR485. The presence of interactions with residues at both the binding cavity and adjacent regions highlights the robust binding profile of TES7832, further supporting its candidacy as a potent binder. The robustness of this binding was further validated through molecular dynamics simulations, which demonstrated stable ligand interactions and minimal fluctuations over a 100 ns simulation period. The maintenance of hydrogen bonds throughout the trajectory further highlighted the stability of the TMPRSS2:TES7832 complex. The binding free energy estimation using MMPBSA analysis provided additional support for the strong and stable interaction between TES7832 and TMPRSS2, with a favorable Gibbs free energy. This binding energy underscores the potential of TES7832 as an effective inhibitor of TMPRSS2.

The uniqueness of this study lies in targeting the SRCR domain of TMPRSS2, an underexplored therapeutic site that plays a crucial role in the formation of the *TMPRSS2/ERG* fusion in prostate cancer [23]. By identifying TES7832 as a lead compound with stable binding at the SRCR domain and favorable drug-like properties, this study sets the stage for further experimental validation and development of targeted therapies aimed at disrupting the *TMPRSS2/ERG* fusion axis in PC.

TES7832 inhibited the cell-free TMPRSS2 activity, which was consistent with the observed computational analysis. The effect of TES7832 was then checked on the proliferation of two cell lines, VCaP and the LNCaP, that express native TMPRSS2. The compound effectively inhibited the proliferation of the VCaP cells but did not affect LNCaP proliferation. While both these cells express the native TMPRSS2, only VCaP possesses the *TMPRSS2/ERG* gene fusion [7,24]. We therefore reasoned that TES7832 targeted the *TMPRSS2/ERG* instead of the native TMPRSS2. To elucidate the specificity, we tested the effect of TES7832 on HUVEC cells that express *ERG*. The compounds did

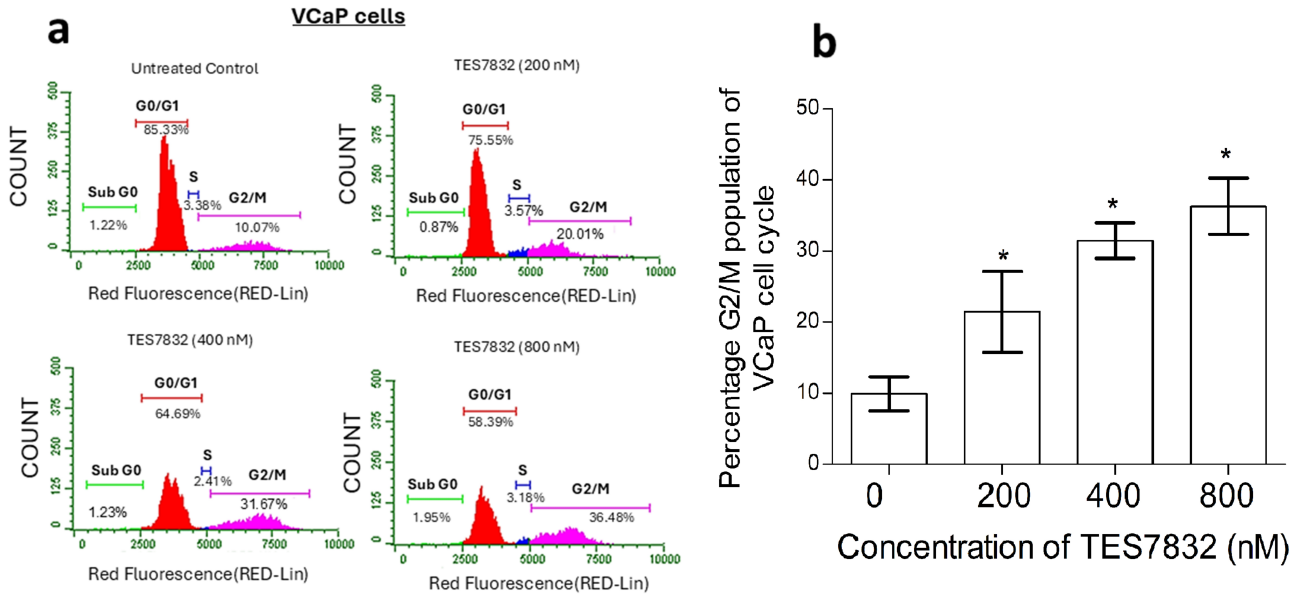

Fig. 12. Effects of TES7832 on VCaP cell cycle. At 72 hours of treatment, the TES7832 promoted G_2/M cell cycle Arrest in VCaP cells. (a) Representative graphs of the cell cycle assay depicting the population of VCaP cells at different cell cycle stages when treated with TES7832 doses. (b) Histograms represent the dose-dependent efficacy of TES7832 in inducing G_2/M cell cycle arrest in the VCaP cells. All tests were conducted three times, and representative results were provided. The results are expressed as mean ± SD and are statistically significant at $*p < 0.05$.

not affect the cell viability of HUVEC cells at a very high concentration compared to the GI_{50} value of VCaP cells. TES7832 exhibited a higher therapeutic index since it did not affect normal prostate cell viability at many folds of the GI_{50} value in VCaP cells.

To find the mechanistic pathway, the endogenous *ERG* expression was studied in the VCaP cells with TES7832 treatment. The compound dose-dependently reduced the *ERG*-positive populations in these cells. To eliminate other routes of *ERG* attenuation by the compound, *ERG*-positive populations in HUVEC cells were analyzed. HUVEC cells are positive for *ERG* but negative for TMPRSS2 [25]. The compound showed no effect in the *ERG* levels of HUVEC cells, confirming the *ERG* attenuation was mediated by the TMPRSS2.

We also assessed the impact of TES7832 on endogenous AR in hormone-responsive prostate cancer cell lines, as ERG expression in the TMPRSS2 environment is dependent on AR [25]. For this, the VCaP cells (which are positive for the *TMPRSS2/ERG* and AR), LNCaP cells (that express native TMPRSS2 and AR but do not possess the *TMPRSS2/ERG* gene fusion), and the HUVEC cells (which are negative for TMPRSS2 but possess the native *ERG* and AR) were tested with TES7832 treatments. TES7832 dose-dependently decreased the AR-positive populations only in VCaP, but no significant effect was observed in the LNCaP or the HUVEC cells. This was consistent with the *in vitro* data, where the compound inhibited the proliferation of the VCaP cells but did not alter the viability of LNCaP or the HUVEC cells. Therefore, it is evident that TES7832 is a selective inhibitor of the *TMPRSS2/ERG* fusion, sparing other routes of endogenous *ERG* or AR levels.

Next, to elucidate the mode of cell death, we analyzed the apoptosis with TES7832 treatment. A dose-dependent effect of apoptosis induction was observed. HGF has a significant role in *TMPRSS2/ERG*-mediated cell invasion and metastasis. Studies report that HGF activated by TMPRSS2 promoted c-Met receptor tyrosine kinase signaling and initiated a pro-invasive epithelial-mesenchymal transition (EMT) phenotype [24,26,27]. Chemical library screening revealed a potent bioavailable TMPRSS2 inhibitor that inhibited prostate cancer spread *in vivo* [24]. Consistent with the aforementioned observations, when the compound was evaluated on the HGF-induced migration of VCaP cells, a dose-dependent efficacy of the migration inhibition was observed.

To more fully demonstrate the rationality of targeting the *TMPRSS2/ERG* fusion in prostate cancer, it is important to incorporate studies that highlight the functional significance of the *ERG* erythroblast transformation-specific (ETS) DNA-binding domain in mediating oncogenic signaling [5]. This domain plays a central role by interacting with cofactors such as bromodomain-containing protein 4 (BRD4), androgen receptor (AR), and enhancer of zeste homolog 2 (EZH2), thereby reprogramming transcription and promoting tumor progression through pathways like EMT, proliferation, and invasion [28]. Including recent evidence on therapeutic strategies, such as small molecule inhibitors, PROTACs, and peptidomimetics, that directly target this domain will help validate its role as a druggable and mecha-

nistically justified target in *TMPRSS2/ERG*-driven prostate cancer [29]. Compared to existing TMPRSS2 protease inhibitors such as Camostat, which primarily target the serine protease domain and are designed to block viral entry mechanisms (e.g., SARS-CoV-2), TES7832 offers a distinct advantage by selectively targeting the SRCR domain implicated in *TMPRSS2/ERG* fusion-driven oncogenic signaling [30,31]. This domain-specific inhibition may thus provide a more tumor-selective therapeutic strategy, minimizing systemic protease inhibition and potentially reducing off-target effects associated with broader serine protease inhibitors [32]. A potential limitation of this study is the lack of *in vivo* validation to confirm the therapeutic efficacy and pharmacokinetic profile of TES7832 in a physiologically relevant model. Additionally, the specificity of TES7832 toward the SRCR domain of *TMPRSS2/ERG* fusion protein requires further assessment to rule out off-target effects on other SRCR-containing proteins.

Conclusion

To summarize, TES7832 was identified as a promising and selective inhibitor of TMPRSS2 by targeting its SRCR domain, using a combination of high-throughput virtual screening and molecular dynamics simulations. This domain plays a critical role in the structural and functional integrity of the *TMPRSS2/ERG* fusion protein. Functional assays demonstrated that TES7832 significantly inhibited proliferation and migration, while promoting apoptosis in prostate cancer cells harboring the *TMPRSS2/ERG* gene fusion, with minimal effects on fusion-negative cells, highlighting its selectivity. These findings provide a compelling rationale for the continued development of TES7832 and its structural analogs as targeted therapies for *TMPRSS2/ERG*-driven prostate cancer. However, comprehensive *in vivo* studies are warranted to evaluate its pharmacokinetics, efficacy, and safety in preclinical models.

Availability of Data and Materials

All data were used in this study and any supporting information is available from the corresponding author upon reasonable request.

Author Contributions

Conceptualization, methodology, validation, formal analysis, writing, and funding acquisition: AD and MF. Both authors were involved in the drafting and critical revision of the manuscript. Both authors have read and approved the final manuscript. Both authors have participated sufficiently in the work and agreed to be accountable for all aspects of the work.

Ethics Approval and Consent to Participate

Not applicable.

Acknowledgment

Not applicable.

Funding

The authors extend their appreciation to the Deanship of Scientific Research at King Khalid University for funding this work through a large group Research Project under grant number (RGP2/154/46).

Conflict of Interest

The authors declare no conflict of interest.

References

[1] Wang L, Lu B, He M, Wang Y, Wang Z, Du L. Prostate Cancer Incidence and Mortality: Global Status and Temporal Trends in 89 Countries From 2000 to 2019. Frontiers in Public Health. 2022; 10: 811044. https://doi.org/10.3389/fpubh.2022.811044.

[2] Posdzich P, Darr C, Hilser T, Wahl M, Herrmann K, Hadaschik B, *et al*. Metastatic Prostate Cancer-A Review of Current Treatment Options and Promising New Approaches. Cancers. 2023; 15: 461. https://doi.org/10.3390/cancers15020461.

[3] Sumanasuriya S, De Bono J. Treatment of Advanced Prostate Cancer-A Review of Current Therapies and Future Promise. Cold Spring Harbor Perspectives in Medicine. 2018; 8: a030635. https://doi.org/10.1101/cshperspect.a030635.

[4] St John J, Powell K, Conley-Lacomb MK, Chinni SR. TMPRSS2-ERG Fusion Gene Expression in Prostate Tumor Cells and Its Clinical and Biological Significance in Prostate Cancer Progression. Journal of Cancer Science & Therapy. 2012; 4: 94–101. https://doi.org/10.4172/1948-5956.1000119.

[5] Wang Z, Wang Y, Zhang J, Hu Q, Zhi F, Zhang S, *et al*. Significance of the TMPRSS2:ERG gene fusion in prostate cancer. Molecular Medicine Reports. 2017; 16: 5450–5458. https://doi.org/10.3892/mmr.2017.7281.

[6] Sun C, Dobi A, Mohamed A, Li H, Thangapazham RL, Furusato B, *et al*. TMPRSS2-ERG fusion, a common genomic alteration in prostate cancer activates C-MYC and abrogates prostate epithelial differentiation. Oncogene. 2008; 27: 5348–5353. https://doi.org/10.1038/onc.2008.183.

[7] Chen YW, Lee MS, Lucht A, Chou FP, Huang W, Havighurst TC, *et al*. TMPRSS2, a serine protease expressed in the prostate on the apical surface of luminal epithelial cells and released into semen in prostasomes, is misregulated in prostate cancer cells. The American Journal of Pathology. 2010; 176: 2986–2996. https://doi.org/10.2353/ajpath.2010.090665.

[8] Stopsack KH, Su XA, Vaselkiv JB, Graff RE, Ebot EM, Pettersson A, *et al*. Transcriptomes of Prostate Cancer with TMPRSS2:ERG and Other ETS Fusions. Molecular Cancer Research: MCR. 2023; 21: 14–23. https://doi.org/10.1158/1541-7786.MCR-22-0446.

[9] Pettersson A, Graff RE, Bauer SR, Pitt MJ, Lis RT, Stack EC, *et al*. The TMPRSS2:ERG rearrangement, ERG expression, and prostate cancer outcomes: a cohort study and meta-analysis. Cancer Epidemiology, Biomarkers & Prevention: a Publication of the American Association for Cancer Research, Cosponsored

by the American Society of Preventive Oncology. 2012; 21: 1497–1509. https://doi.org/10.1158/1055-9965.EPI-12-0042.

[10] Barwick BG, Abramovitz M, Kodani M, Moreno CS, Nam R, Tang W, *et al*. Prostate cancer genes associated with TMPRSS2-ERG gene fusion and prognostic of biochemical recurrence in multiple cohorts. British Journal of Cancer. 2010; 102: 570–576. https://doi.org/10.1038/sj.bjc.6605519.

[11] Strobelt R, Adler J, Shaul Y. The Transmembrane Protease Serine 2 (TMPRSS2) Non-Protease Domains Regulating Severe Acute Respiratory Syndrome Coronavirus 2 (SARS-CoV-2) Spike-Mediated Virus Entry. Viruses. 2023; 15: 2124. https://doi.org/10.3390/v15102124.

[12] Novakowski KE, Huynh A, Han S, Dorrington MG, Yin C, Tu Z, *et al*. A naturally occurring transcript variant of MARCO reveals the SRCR domain is critical for function. Immunology and Cell Biology. 2016; 94: 646–655. https://doi.org/10.1038/icb.2016.20.

[13] Barros de Lima G, Nencioni E, Thimoteo F, Perea C, Pinto RFA, Sasaki SD. TMPRSS2 as a Key Player in Viral Pathogenesis: Influenza and Coronaviruses. Biomolecules. 2025; 15: 75. https://doi.org/10.3390/biom15010075.

[14] Farooqi AA, Hou MF, Chen CC, Wang CL, Chang HW. Androgen receptor and gene network: Micromechanics reassemble the signaling machinery of TMPRSS2-ERG positive prostate cancer cells. Cancer Cell International. 2014; 14: 34. https://doi.org/10.1186/1475-2867-14-34.

[15] Valdés-Tresanco MS, Valdés-Tresanco ME, Valiente PA, Moreno E. gmx_MMPBSA: A New Tool to Perform End-State Free Energy Calculations with GROMACS. Journal of Chemical Theory and Computation. 2021; 17: 6281–6291. https://doi.org/10.1021/acs.jctc.1c00645.

[16] Swanson K, Walther P, Leitz J, Mukherjee S, Wu JC, Shivnaraine RV, *et al*. ADMET-AI: a machine learning ADMET platform for evaluation of large-scale chemical libraries. Bioinformatics (Oxford, England). 2024; 40: btae416. https://doi.org/10.1093/bioinformatics/btae416.

[17] Abohassan M, Al Shahrani M, Ahmad I, Abullais SS, Srivastava S, Rajagopalan P. GC/MS characterization and computational kinome-wide screening of pomegranate fruit extract identifies key phytochemicals interacting to CDK kinases implicated in acute myeloid leukemia cells. Journal of Food Biochemistry. 2022; 46: e14178. https://doi.org/10.1111/jfbc.14178.

[18] Belkahla S, Nahvi I, Biswas S, Nahvi I, Ben Amor N. Advances and development of prostate cancer, treatment, and strategies: A systemic review. Frontiers in Cell and Developmental Biology. 2022; 10: 991330. https://doi.org/10.3389/fcell.2022.991330.

[19] Demichelis F, Fall K, Perner S, Andrén O, Schmidt F, Setlur SR, *et al*. TMPRSS2:ERG gene fusion associated with lethal prostate cancer in a watchful waiting cohort. Oncogene. 2007; 26: 4596–4599. https://doi.org/10.1038/sj.onc.1210237.

[20] Nam RK, Sugar L, Yang W, Srivastava S, Klotz LH, Yang LY, *et al*. Expression of the TMPRSS2:ERG fusion gene predicts cancer recurrence after surgery for localised prostate cancer. British Journal of Cancer. 2007; 97: 1690–1695. https://doi.org/10.1038/sj.bjc.6604054.

[21] Fraser BJ, Beldar S, Seitova A, Hutchinson A, Mannar D, Li Y, *et al*. Structure and activity of human TMPRSS2 protease implicated in SARS-CoV-2 activation. Nature Chemical Biology. 2022; 18: 963–971. https://doi.org/10.1038/s41589-022-01059-7.

[22] Wilson S, Greer B, Hooper J, Zijlstra A, Walker B, Quigley J, *et al*. The membrane-anchored serine protease, TMPRSS2, activates PAR-2 in prostate cancer cells. The Biochemical Journal. 2005; 388: 967–972. https://doi.org/10.1042/BJ20041066.

[23] Tomlins SA, Laxman B, Varambally S, Cao X, Yu J, Helgeson BE, *et al*. Role of the TMPRSS2-ERG gene fusion in prostate cancer. Neoplasia (New York, N.Y.). 2008; 10: 177–188. https://doi.org/10.1593/neo.07822.

[24] Lucas JM, Heinlein C, Kim T, Hernandez SA, Malik MS, True LD, *et al*. The androgen-regulated protease TMPRSS2 activates a proteolytic cascade involving components of the tumor microenvironment and promotes prostate cancer metastasis. Cancer Discovery. 2014; 4: 1310–1325. https://doi.org/10.1158/2159-8290.CD-13-1010.

[25] Mohamed AA, Xavier CP, Sukumar G, Tan SH, Ravindranath L, Seraj N, *et al*. Identification of a Small Molecule That Selectively Inhibits ERG-Positive Cancer Cell Growth. Cancer Research. 2018; 78: 3659–3671. https://doi.org/10.1158/0008-5472.CAN-17-2949.

[26] Bottaro DP, Rubin JS, Faletto DL, Chan AM, Kmiecik TE, Vande Woude GF, *et al*. Identification of the hepatocyte growth factor receptor as the c-met proto-oncogene product. Science (New York, N.Y.). 1991; 251: 802–804. https://doi.org/10.1126/science.1846706.

[27] Ko CJ, Hsu TW, Wu SR, Lan SW, Hsiao TF, Lin HY, *et al*. Inhibition of TMPRSS2 by HAI-2 reduces prostate cancer cell invasion and metastasis. Oncogene. 2020; 39: 5950–5963. https://doi.org/10.1038/s41388-020-01413-w.

[28] Fu J, Zhang J, Chen X, Liu Z, Yang X, He Z, *et al*. ATPase family AAA domain-containing protein 2 (ATAD2): From an epigenetic modulator to cancer therapeutic target. Theranostics. 2023; 13: 787–809. https://doi.org/10.7150/thno.78840.

[29] An S, Fu L. Small-molecule PROTACs: An emerging and promising approach for the development of targeted therapy drugs. EBioMedicine. 2018; 36: 553–562. https://doi.org/10.1016/j.ebiom.2018.09.005.

[30] Mahoney M, Damalanka VC, Tartell MA, Chung DH, Lourenço AL, Pwee D, *et al*. A novel class of TMPRSS2 inhibitors potently block SARS-CoV-2 and MERS-CoV viral entry and protect human epithelial lung cells. Proceedings of the National Academy of Sciences of the United States of America. 2021; 118: e2108728118. https://doi.org/10.1073/pnas.2108728118.

[31] Hoffmann M, Hofmann-Winkler H, Smith JC, Krüger N, Arora P, Sørensen LK, *et al*. Camostat mesylate inhibits SARS-CoV-2 activation by TMPRSS2-related proteases and its metabolite GBPA exerts antiviral activity. EBioMedicine. 2021; 65: 103255. https://doi.org/10.1016/j.ebiom.2021.103255.

[32] Sananes A, Cohen I, Allon I, Ben-David O, Abu Shareb R, Yegodayev KM, *et al*. Serine protease inhibitors decrease metastasis in prostate, breast, and ovarian cancers. Molecular Oncology. 2023; 17: 2337–2355. https://doi.org/10.1002/1878-0261.13513.